3E analysis of a biomass-to-liquids production system based on solar gasification

Dian Zhong, Kuo Zeng, Jun Li, Xinyi Yang, Yang Song, Youjian Zhu, Gilles Flamant, Ange Nzihou, Haiping Yang, Hanping Chen

3E analysis of a biomass-to-liquids production system based on solar gasification

Dian Zhong[a], Kuo Zeng[a,b,] Jun Li[a], Xinyi Yang[a], Yang Song[a], Youjian Zhu[a], Gilles Flamant[c], Ange Nzihou[d], Haiping Yang[a], Hanping Chen[a]

[a]State Key Laboratory of Coal Combustion, Huazhong University of Science and Technology, 1037 Luoyu Road, Wuhan, Hubei 430074, PR China

[b]Shenzhen Huazhong University of Science and Technology Research Institute, Shenzhen, 523000, China

[c]Processes, Materials and Solar Energy Laboratory, PROMES-CNRS, 7 rue du Four Solaire, 66120 Odeillo Font Romeu, France

[d]Université de Toulouse, Mines Albi, UMR CNRS 5302, Centre RAPSODEE, Campus Jarlard, F-81013 Albi cedex 09, France

Abstract

The solar gasification system (SGS) and traditional system are modeled by Aspen Plus. And their energetic, economic as well as ecologic (3E) performance are compared. The effects of different feedstocks and Direct Normal Irradiance (DNI) to the productivity and efficiency of SGS are also carried out. The results show that a biomass-based, solar-assisted liquid fuel production system offers a productivity increasing potential of 49.44% more refined syngas and 65.74% more liquid fuels due to its higher utilization of feedstock. And for the same reason, the energetic performance of SGS increases from 40.22% to 40.66% for thermal efficiency and from 38.35% to 41.35% for exergy efficiency compared with those of reference

system. The final price of products in SGS could only be equal to that of reference system when the carbon tax is under considering, while both of them shows no superiority to that of petroleum products. SGS has a better ecology performance contributed by less total carbon and water footprints which are only 55.27% and 61.34% of those of the reference system.

Key words: Biomass-to-liquid; Gasification; Solar energy; 3E analysis

1. Introduction

The demand for liquid fuel is increasing rapidly for long-distance transport, with fuel consumption of about 580,000 barrels per day in 2019, and it is excepted to grow continually [1]. The consumed fuel derived from the petroleum products released a lot of greenhouse gas and negative gas like CO_2 and NO_X when combusted, which is harmful to environment. Therefore, it is urgent and necessary to find a method to obtain liquid fuel with more ecologic benefits while achieving higher efficiency and better economic benefit competitive with traditional techniques. To achieve this purpose, biomass is proposed to be a promising carbon feedstock for liquid fuel production.

Biomass gasification has been proved to be an attractive approach for liquid fuel production [2–4]. Large quantities of syngas are produced in this gasification reaction, and the syngas can be further synthesized to liquid fuel through suitable catalytic processes like Fischer-Tropsch (F-T) process [5]. However, traditional autothermal gasification systems require additional heat to drive the endothermic reactions by burning about 20-30% of the feedstock[6]. It results in the syngas contamination with

combustion products and the low utilization rate of feedstock that further decreases the gasification efficiency (the ratio of total low heating value of syngas products to that of feedstock) [7]. To overcome these drawbacks, solar energy has been explored as an alternatives of traditional heat source driving the gasification process [8–11].

The productivity of syngas as well as liquid fuel usually increases with the assistance of solar energy. Kaniyal et al [12] obtained a higher total annually averaged energetic productivity of 21% for a coal-to-liquid system with solar gasification comparing with tradition system. Hathaway et al. established a biomass gasification system with concentrated solar power of 100 MW, the annual average thermal efficiency reached up to 82% superior to that of the traditional gasification system [6,13,14]. Though the system using biomass as feedstock is found to have better ecologic potential [15], its total cost and price are still not competitive enough with that of conventional refinery [16]. Recent researches have reported that solar system is expected to become economically competitive in the near future based on the larger scale of production and expected reduction in the cost of subsystems [17]. Considering that the fuel prices will fluctuate with its investment and overall cost of a certain system, the economic performance of a solar gasification system (SGS) remains unknown. Consequently, the economic performance of SGS in different situations should be further investigated [18,19]. As for the ecological impact, the participation of solar energy significantly reduces the CO_2 emission in gasification process without burning the feedstock. But there are still additional indirect emission and consumption accompany with the extra facilities of solar system, which causes

the ecologic performance of solar driven system unclear.

Therefore, the 3E analysis of a biomass-to-liquids production system based on solar gasification was carried out in this paper. Aspen Plus is used to model the SGS and the reference system to analyze their total net efficiency of thermal and exergy as well as their productivity. Besides, the performance of SGS under different feedstocks and DNI is estimated. And the economic performance was discussed by estimating the system cost and products' price as well the sensitivity. Finally, the ecological footprint was analyzed to indicate the ecological influences on the environment.

2. System

2.1 Flow chart and boundary

The transience and intermittent of solar energy are harmful to the liquid hydrocarbon fuel synthesis process because the FT reactor is very sensitive to the variations during system operation. So, the solar gasification system is designed to be consisted by three subsystems named solar gasification, fuel synthesis system and syngas storage system. Syngas storage system can not only smooth the fluctuations in upstream, e.g., fluctuation caused by the transience of solar energy, but also reserve enough syngas in case of a long period without sunlight like rainy days or dark nights. A traditional gasification system that has the same structure with SGS except using less storage tanks and replacing solar collection section with air separation is proposed to make a comparison. The flow charts of two systems are shown in **Error! Reference source not found.**.

The boundary of whole process of biomass utilization is divided into four steps

depicted in Fig 2 for analyzing the ecology performance of two system. The boundary shows each part of this process affects the environment in both direct and indirect ways, such as direct exhaust emission and indirect fuel consumption during biomass transportation.

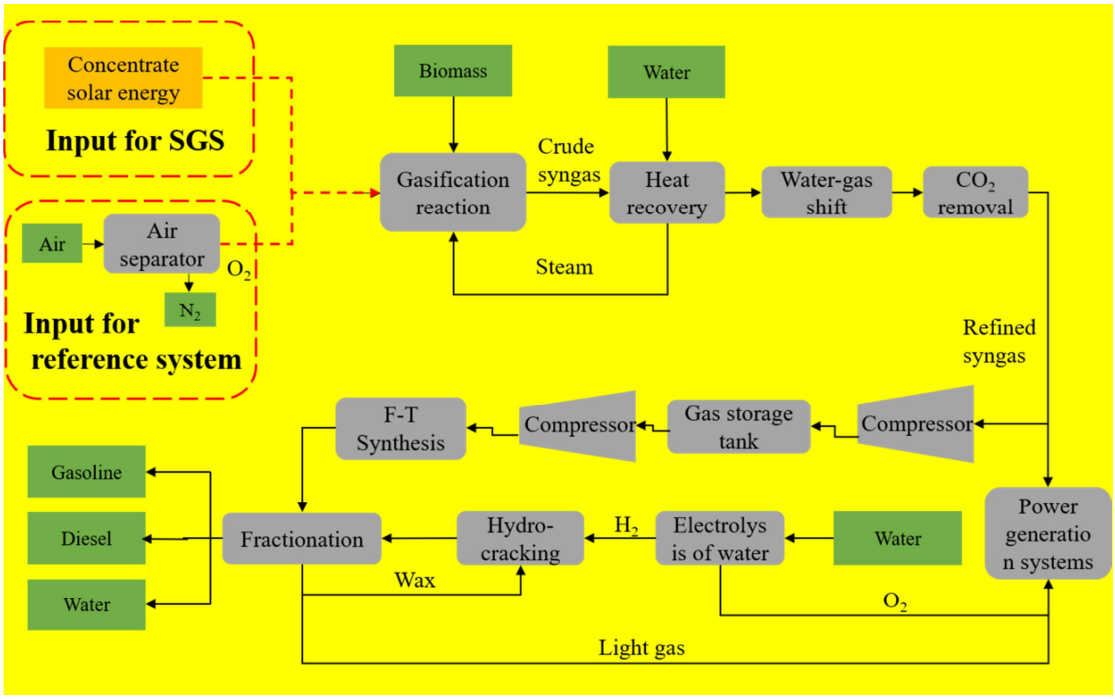

Fig 1. Flow chart of SGS and reference system

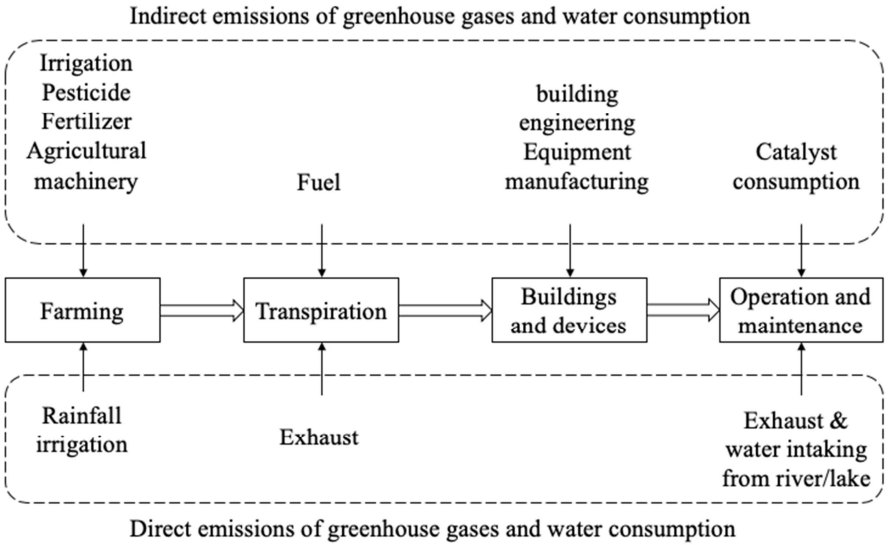

Fig 2. Boundary of fuel synthesis system

2.2 Reaction conditions

Biomass gasification with steam includes complex chemical reactions. The main reactions that are related to gasification process are listed in Table 1.

Table 1. Reactions in gasification process [8,18,20]

Name	Reactions	number
Steam gas shift reaction	$C+H_2O=CO+H_2,\ \Delta H_{25℃}=131\ kJ/mol$	(1)
Boudouard reaction	$C+CO_2=2CO,\ \Delta H_{25℃}=172\ kJ/mol$	(2)
Methanation Reaction	$C+2H_2=CH_4,\ \Delta H_{25℃}=-75\ kJ/mol$	(3)
Methane refined	$CH_4+H_2O=CO+3H_2,\ \Delta H_{25℃}=206\ kJ/mol$	(4)
Water-gas shift	$CO+H_2O=CO_2+H_2,\ \Delta H_{25℃}=-42\ kJ/mol$	(5)

The ideal overall reaction of steam gasification of biomass can be described by Eq(6).

$$C_1H_xO_y+(1-y)H_2O=CO+\left(1-y+\frac{x}{2}\right)H_2 \quad (6)$$

where x and y respectively represent the H/C and O/C of biomass materials. This gasification reaction tends to increase in volume, which is not conducive to gas production. Thus, the pressure of gasification reaction is set at 1 bar in this paper.

Xinjiang, China has abundant solar resource and is widely planted with cotton, which is suitable for solar gasification. Therefore, the cotton stock was selected as feedstock. And the proximate analysis of the air-dried cotton stock was 80.785%

volatile, 2.686 wt% ash, 11.004 wt% fixed carbon, and 5.525 wt% moisture. The elemental composition of the dried feedstock was 45.011 wt% carbon, 6.094 wt% hydrogen, 40.040 wt% oxygen, and 0.601 wt% nitrogen. Its low heating value reached 17564.80 kJ/kg [21]. Based on the characteristics of cotton straw samples and Eq(6), the theoretical value of the ratio of steam to biomass (S/B) for gasification reaction is 0.25. however, the ratio needs to be adjusted to a specific range which is generally higher than 2, resulting extra water input. Therefore, the S/B changes with different feedstock and reaction conditions.

3. Methodology and data

3.1 System modeling

The solar gasification sub-system, fuel synthesis sub-system and other important devices had been modeled. Those other important devices include syngas storage facilities, power generation equipment and auxiliary equipment used in both systems.

3.1.1 Solar gasification sub-system

In the gasification reactor, the biomass feedstock and steam were heated by concentrated solar energy to produce crude syngas. The theoretical heat absorption of the reaction process $\dot{Q}_{gasification,net}$ is:

$$\dot{Q}_{gasification,net} = \dot{m}_{bio} \Delta h_{gasification,25°C} \quad (7)$$

where $\dot{m}_{bio}$ is mass flow rate of biomass feedstock, kg/s; $\Delta h_{gasification,25°C}$ is net enthalpy change of biomass feedstock gasification reaction per unit mass, which can be defined as follows:

$$\Delta h_{gasification,25°C} = \sum_{i}^{n} n_i h_{i,25°C} - n_{bio} h_{bio,25°C} - n_{H_2O} h_{H_2O,25°C} \quad (8)$$

Where n_i represents the moles of fraction i, mol; $h_{i,25°C}$ represents the standard enthalpy of fraction i at the temperature of 25 °C.

To represent the amount of energy converted into syngas during gasification, the solar energy conversion rate η_{solar} is defined as follows [22]:

$$\eta_{solar} = \frac{\dot{Q}_{gasification,net}}{\dot{Q}_{gasification,net} + \dot{m}_{bio} LHV_{bio}} \quad (9)$$

Where the LHV_{bio} is the low heat value of biomass feedstock.

The actual heat absorption of the biomass gasification with steam $\dot{Q}_{gasification,T}$ is:

$$\dot{Q}_{gasification,T} = \dot{m}_{bio} \Delta h_{gasification,T} \quad (10)$$

Where $\Delta h_{gasification,T}$ represents the total heat absorption of the gasification reaction in certain temperature T; T represents the gasification reaction temperature, °C；The $\Delta h_{gasification,T}$ is defined as:

$$\Delta h_{gasification,T} = \sum_{i}^{n} n_i h_{i,T} - n_{bio} h_{bio,25°C} - n_{H_2O} h_{H_2O,25°C} \quad (11)$$

Where $h_{i,T}$ represents the formation enthalpy of syngas components i at the reaction temperature.

The actual heat absorption of the biomass gasification with steam can also be calculated as：

$$\dot{Q}_{gasification,T} = \dot{Q}_{reactor} \eta_{absorption} \quad (12)$$

where the $\dot{Q}_{reactor}$ represents the energy radiated to the reactor, kW; $\eta_{absorption}$ represents the absorption efficiency of reactor, which can be expressed as [11]:

$$\eta_{absorption}=1-\left(\frac{\sigma T^4}{IC}\right) \quad (13)$$

Where σ represents Steff-Boltzmann constant, W/(m^2K^4); I represents the standard solar intensity, W/m^2; C represents the average concentrating ratio of the concentrated solar energy entering the reactor.

Then the heat loss caused by the reactor is:

$$\dot{Q}_{reactor,loss}=\dot{Q}_{reactor}\left(1-\eta_{absorption}\right) \quad (14)$$

The solar energy from the heliostat field to the gasification reactor can be illustrated as：

$$\dot{Q}_{reactor}=\dot{Q}_{solar}\eta_{opt} \quad (15)$$

where the $\dot{Q}_{solar}$ represents the solar radiation received by the heliostats field, kW; η_{opt} represents the average optical efficiency of the heat collecting system, which can be assumed as 68.6% based on the Hu's study [22]. Then the heat loss caused by the optical characteristics of the heliostat field is:

$$\dot{Q}_{solar,loss}=\dot{Q}_{solar}\left(1-\eta_{opt}\right) \quad (16)$$

Exergy of solar energy is calculated according to the following formula [23]:

$$\dot{E}x_{solar}=\left(1-\frac{T_{ambient}}{T_{sun}}\right)\dot{Q}_{solar} \quad (17)$$

where $T_{ambient}$ represents the ambient temperature, which was set as 25°C; T_{sun} is the temperature on the surface of sun, which is about 5500°C.

Exergy of biomass can be calculated as follows [23]:

$$\dot{E}x_{bio}=\beta_{bio}\dot{m}_{bio}LHV_{bio} \quad (18)$$

where β_{bio} represents the ratio of biomass chemical exergy to lower calorific value,

and is calculated as follows [23]:

$$\beta_{bio}=1.0437+0.1882\left(\frac{m_H}{m_C}\right)+0.0661\left(\frac{m_O}{m_C}\right)+0.0404\left(\frac{m_N}{m_C}\right) \quad (19)$$

where m_C, m_H, m_O and m_N represent the elemental mass ratio of C, H, O and N in the biosmass materials.

The ratio of H_2 to CO in the crude syngas obtained from gasification reaction needs to be adjusted by water-gas shift reaction described as Eq (5). The reaction releases heat of 42kJ per mole of CO, and the heat released by water gas conversion reaction is:

$$Q_{WGS}=42\times\dot{n}_{CO} \quad (20)$$

where $\dot{n}_{CO}$ is the mole flow rate of CO taken into reaction.

Pressure Swing Adsorption (PSA) technology was applied to remove the CO_2 in the syngas to meet the requirement for fuel synthesis. The energy consumption of the process of CO_2 removal by PSA is calculated according to the following formula[24]

$$W_{PSA}=-RT_{PSA}\left[\sum_i^n n_{i,P}\ln\left(\frac{y_{i,P}}{y_{i,F}}\right)+\sum_j^n n_{j,P}\ln\left(\frac{y_{j,E}}{y_{j,F}}\right)\right] \quad (21)$$

where $y_i=\frac{n_i}{\sum_i^n n_i}$ represents the proportion of one component in the mixture of gases; the subscripts F, P and E represent feedstock, product and exhaust respectively. The recovery rate of PSA is about 90% [24], thus some H_2 and CO will be released into the exhaust gas.

3.1.2 Fuel synthesis sub-system

The syngas produced from solar gasification is processed through a series of processes. Some of syngas is injected into the F-T reactor, while the rest is stored in the gas storage tank. Before entering the F-T reactor, the syngas needs to be pressurized by a compressor to the reaction pressure required by the F-T reaction, which is expressed as follow:

$$\left(2n+1\right)H_2+nCO=C_nH_{2n+2}+nH_2O \tag{22}$$

The yields of hydrocarbon products with different carbon atom numbers satisfied the Anderson-Schulz-Flory distribution [17], and the formula is as follows:

$$M_n=na^{n-1}\left(1-a\right)^2 \tag{23}$$

where n is the number of carbon atoms in hydrocarbon products; M_n is the mass fraction of hydrocarbons with n carbon atoms in hydrocarbon products; α is the growth probability of carbon chain, whose value is related to the operating conditions of F-T reaction and the composition of fed syngas.

The F-T reaction is reported to produce more hydrocarbons that contain more than five carbon atoms (especially wax) at a lower reaction temperature. And the cobalt-based catalyst will also have a better performance for F-T reaction in this condition [25]. Therefore, the F-T synthesis in these systems was conducted at a temperature of 220°C and pressure of 20 bar, producing 8.15% light gas, 29.72% gasoline, 28.21% diesel and 33.92% wax. The α is 0.9 [26] and the CO conversion rate reaches 90% [27] in this case.

Waxes can be further hydrocracked to produce hydrocarbons with shorter carbon

chains like gasoline and diesel. The yields of hydrocarbons derived from hydrocracking process with platinum-based catalyst were 3.77wt% for light gas, 61.19wt% for gasoline, 27.04% for diesel, 8.00% for wax remained when the temperature is 330°C and the pressure is 35 bar while the mass ratio of H_2 to waxes is 0.1 [28].

H_2 required for hydrocracking is produced by electrolysis of water. In this paper, an improved acid/alkaline amphoteric water electrolysis (AAEC) technology [29] is used to provide H_2 for hydrocracking to obtain higher system efficiency.

The electric power consumed during water electrolysis is:

$$W_{AAEC}=\dot{V}_{H_2}E_{AAEC} \tag{24}$$

where $\dot{V}_{H_2}$ is the volume flow rate of H_2, m^3/s; E_{AAEC} is the energy comsumption producing H_2 per unit volume, which is reported to be 2.85 kWh/m^3 [29].

3.1.3 Other devices

A compressor is needed to compress the refined syngas for storage. The gas storage pressure is set at 5 bar. The energy consumption of compressor will be calculated with the isentropic compressor model in Aspen Plus as the isentropic efficiency and the mechanical efficiency set at 0.88 [30,31] and 0.9 [32], respectively.

The light gas from the fuel synthesis process will be used to drive the gas-steam combined cycle for electricity generation to meet the system's electrical load, with syngas making up the shortfall. Since the power generation is not the main point, the thermal efficiency of the combined cycle based on the LHV of fuel can be set at 55% according to the results in other researches [33,34] and the power generation and heat

release of the combined cycle are calculated by follows respectively:

$$W_{CC} = \eta_{CC} \dot{n}_{fuel} LHV_{fuel} \tag{25}$$

$$\dot{Q}_{CC} = (1-\eta_{CC}) \dot{n}_{fuel} LHV_{fuel} \tag{26}$$

where $\dot{n}_{fuel}$ is the mole flow rate of fuel, mol/s; LHV_{fuel} is the low heat value of fuel, kJ/kg; η_{CC} is the efficiency of the combined system.

3.2 Thermodynamic analysis

3.2.1 Gasification efficiency

The efficiency of solar gasification $\eta_{gasification}$ can be defined as [35]:

$$\eta_{gasification} = \frac{LHV_{syngas}}{Q_{reactor} + m_{bio} LHV_{bio}} \tag{27}$$

The molar fraction of gasification products under different temperatures are shown in Fig 3. It indicates that the molar ratio of H_2 and CO increases rapidly with the increase of gasification reaction temperature, and tends to be stable after 900°C, eventually reaching 53.21% and 46.54% respectively. On the contrary, the H_2/CO ratio decrease as temperature rising, and gradually stabilize at 1.14 as shown in Fig 4. The sum of molar ratios of other gas components is less than 1%. And the gasification reaction can be considered finished. In Fig 5, the gasification efficiency of SGS has been studied under different temperatures. And there is a peak of gasification efficiency of 85.81% at 900°C, which is in accordance with Hathaway's results [36].

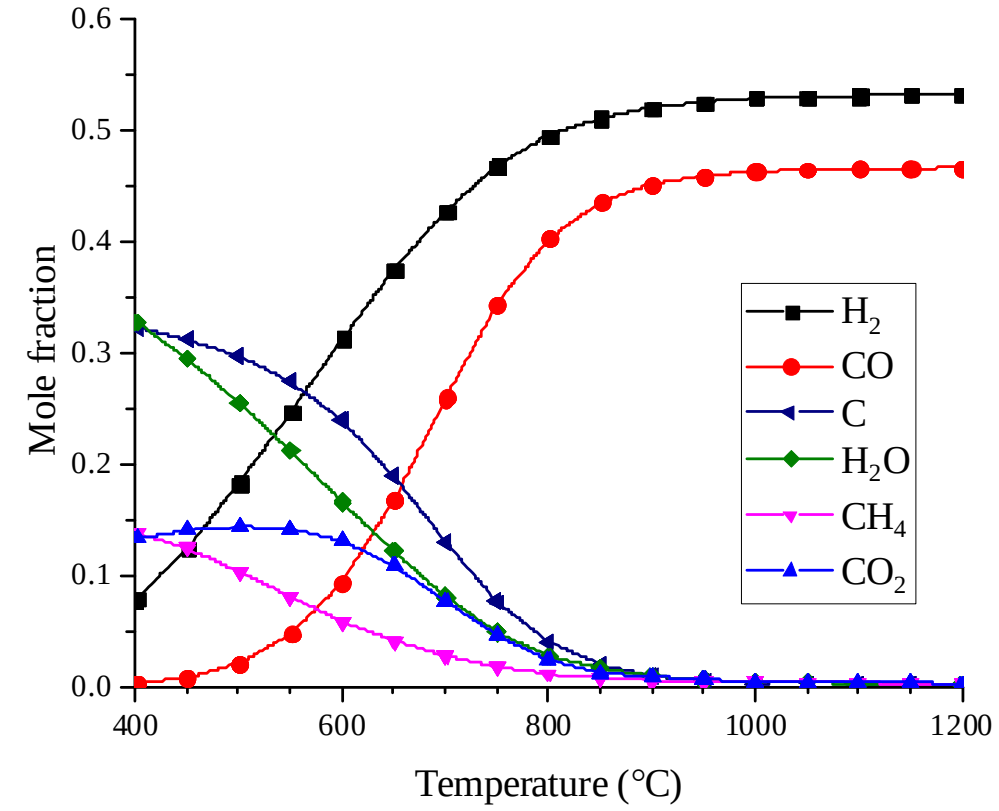

Fig 3. Molar fraction of gasification products under different temperatures

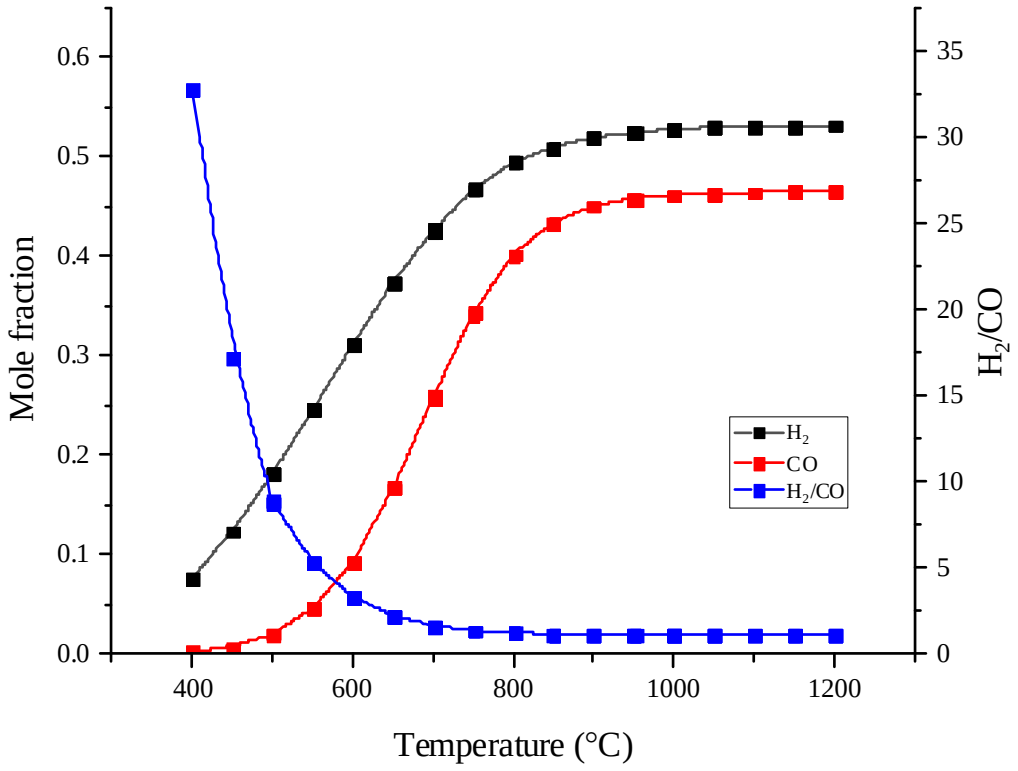

Fig 4. The H_2/CO ratio and the mole fraction of H_2 and CO

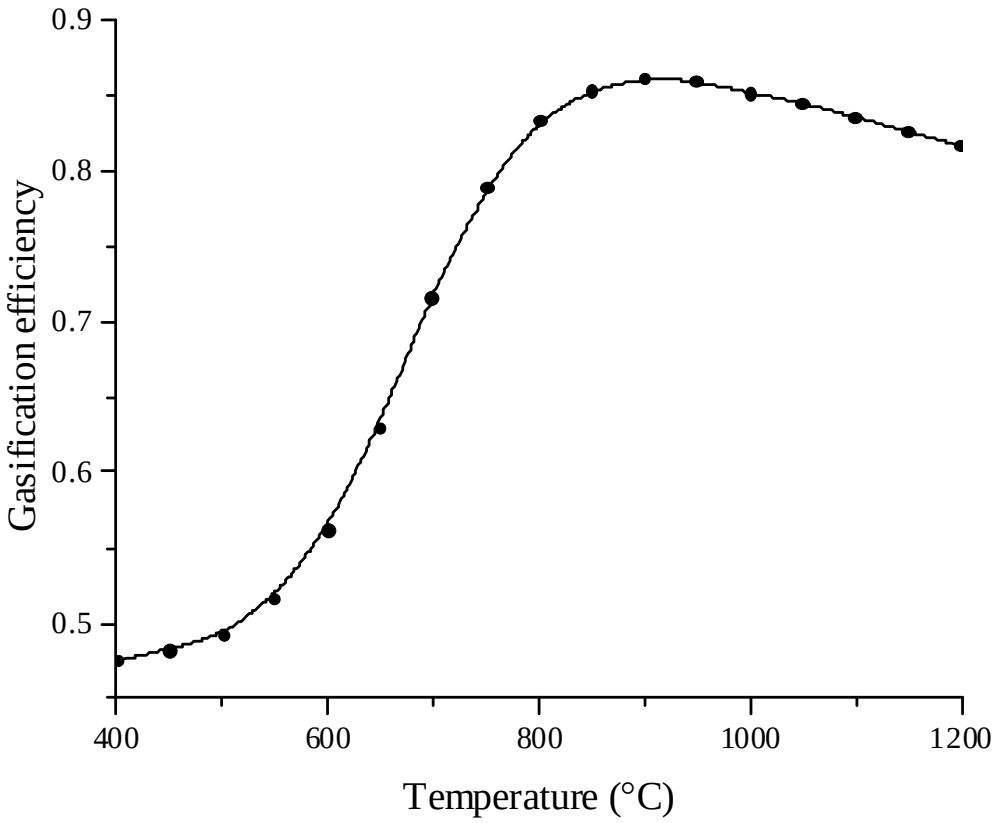

Fig 5. Gasification efficiency at different temperatures.

3.2.2 Material flow

As descripted by Eq(7)-Eq(27), these two systems were modeled and simulated with Aspen Plus software, in which the input of biomass feedstock was set at 1 kg/s, and operation parameters such as fuel yield and system power consumption were calculated. Particularly, the material flow of two systems were listed in Table 2, and the differences of products yield between two systems intuitively represent their characteristic of productivity.

Table 2. Material flow of each system.

Material	Solar system (kg/s)	Normal system (kg/s)
Biomass	1.000	1.000
Steam	0.525	0.196
Oxygen	0.000	0.466

Refined syngas	0.812	0.543
Hydrogen	0.011	0.006
Light gas	0.090	0.054
Gasoline	0.159	0.096
Diesel	0.114	0.069
Water	0.354	0.214
Exhaust	0.713	1.119

3.2.3 Validation

As long as the H_2/CO ratio in syngas remaining unchanged, the mass fraction of the products derived from FT process won't change according to Eq 22 and Eq 23. Thus it is reasonable to mainly focus on the syngas production from gasification process. In order to check the accuracy of gasification system in predicting the productivity of syngas compositions, the dry gas compositions obtained from the Aspen Plus model is compared against experimental findings by [37] in. As shown in the Fig 6, the experimental data show a strong correlation with the prediction, except for higher fraction of hydrogen and lower fraction of CO. It is because the gasification subsystem in SGS is designed for producing a syngas with a higher H_2/CO ratio that suitable for FT synthesis.

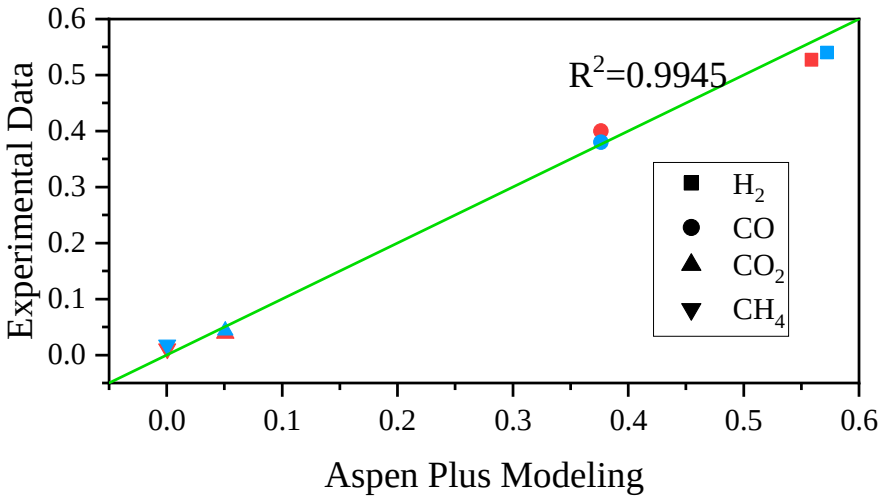

Fig 6. Comparison between the model predictions and experimental findings of the mole fraction (in percentage) of components in syngas:

Red: beech-type A, Blue: Resinous mix-type D. [37]

3.3 Cost of each parts

3.3.1 Cost of heliostat field

Xinjiang in China is rich in solar energy resource; whose solar radiation intensity exceeds 700 W/m^2 in both typical days of summer and winter at noon. In this paper, a solar radiation intensity of 700 W/m^2 was selected as the benchmark to design the heliostat field. The designed power of gasification reactor in both systems is set at 50 MW, on which all subsequent designs of the rest parts of two systems are based.

The System Advisor Model [11] (SAM) platform developed by the Renewable Energy Laboratory of the United States was used for modeling and calculation in the design of heliostat field. According to the solar radiation conditions, the preliminary design of the heliostat field is carried out. The whole heliostat field consists of 886 heliostats, and each single one has an area of 144 m^2, whose total area is 127,584 m^2.

The equipment cost of heliostat field is calculated based on the data given by

SAM platform, and the results showed that the reactor with a designed power of 50MW needs 886 heliostats whose single area is 144 m^2, making up the whole heliostat field with an area of 127584 m^2. And the total cost of this part reached 96.22×10^6 CNY. Based on the designed solar radiation intensity of 700 W/m^2, the annual biomass consumption of SGS is about 5.65×10^4 t/y. The operational conditions of reference system were converted proportionally under the assumption that its liquid fuel output was the same as SGS based on the data shown in Table 2. The annual biomass consumption of reference system was about 9.36×10^4 t/y.

3.3.2 Cost of gas storage tank and heat exchanger

The operation time can be estimated as 6 hours a day. A solar multiple of 3 is adopted, which means that more storage tanks are necessary to support the downstream processes keeping running for at least 16 hours when the syngas production is offline. The cost of storage tanks is related to their material, which is usually carbon steel [38], and their thickness determined by national standard of pressure vessels [39] as 5 bar. According to the container's thickness and capacity, the metal consumption and the cost of a single gas tank is estimated as shown in Appendix Table A1.

The shell and tube heat exchanger can meet the heat exchange requirement of two systems. The heat transfer area of heat exchanger can be calculated as follows:

$$S=\frac{Q}{\Delta TK} \tag{28}$$

where： Q represents the heat load of exchanger, kJ; ΔT represents the logarithmic mean temperature difference, °C; K is heat transfer coefficient.

The cost of heat exchanger, as well as the cooler that is the same with the heat exchanger in structure, is related to the heat exchange surface area. And their correlation can be expressed as the following function [40]:

$$C_{\text{heat exchanger}} = a_1 + a_2 S^{a_3} \quad (29)$$

where the $a_1 = 8000$, $a_2 = 259.2$, $a_3 = 0.91$, as stainless steel was used. The costs of heat exchanger and cooler are calculated as shown in Table 3.

Table 3. The costs of heat exchanger and cooler [40].

		Material type	Heat/cold load (kW)	Heat exchange area (m^2)	Cost (10^6 CNY)
SGS	Heat exchanger	S31020	15511.93	485.88	0.39
	Cooler		8421.43	2338.72	
Reference system	Heat exchanger		5570.95	143.67	0.39
	Cooler		7539.21	2792.58	

3.3.3 Cost of other devices

The main equipment of fuel synthesis system of SGS includes solar heat collection equipment, gasification reactor, water-gas shift reactor, F-T synthesis reactor, water electrolyser, hydrocracking reactor and fractionator, CO_2 removal devices and gas-steam combined cycle power station. Reference systems also require air separation equipment due to the use of oxygen as the main gasifier. The cost of the main equipment can be estimated by relevant literature [17,41–45]. Since the size of the equipment used in the literature is different from what is used in this paper, the cost of these devices can be converted exponentially as follows [26]:

$$C=C_0\left(\frac{S_r}{S_0}\right)^{sf} \quad (30)$$

where C_0 is the cost of the reference equipment; S_r is the capacity of the new equipment; S_0 is the capacity of the reference equipment; sf is the scale factor.

Compressors are needed during the compression of syngas. According to the requirements of the mass flow rate and the import pressure, the four-stage compressor (m-155/55) made by Sichuan Huaxi General Machinery Company was selected, whose cost is 2×10^6 CNY each [32]. A total cost of four compressors was 8×10^6 CNY. Hydrogen required by hydrocracking reaction is provided by water electrolyser. According to the current technical level, the cost of electrolytic water reactor is 7,800 ~ 9,500 CNY/kW [46]. The cost of the water electrolyser is 34.09×10^6 CNY as the load of the electrolyser in the system is 3588.79kW.

3.3.4 Total investment of system

The costs of each parts of the system are shown in Table 4 based on the data given previously and the methods presented in Appendix, Table A2. The operating cost of the whole SGS is consisted of variable cost and fixed cost. Variable costs include biomass raw materials (pretreatment), industrial water, catalysts, etc., and fixed costs include workers' wages, benefits, and system maintenance costs. **Error! Reference source not found.** summarizes the main assumptions used to assess operating costs. The data mainly derived from relevant researches [17,26] and the National Bureau of Statistics [47].

Table 4. Details of investments in two systems

	SGS	Reference system

	10^6 CNY	%	10^6 CNY	%
Solar collector	120.28	18.11		
Air separator			46.12	10.33
Syngas generation	75.46	11.36	125.81	28.19
Syngas storage	189.41	28.52	8.42	1.89
Fuel synthesis	241.55	36.37	241.50	54.11
Auxiliary equipment	37.36	5.63	24.48	5.48
Total fundamental equipment cost	664.06		446.33	
Venues preparation	99.61		66.95	
Service facility	132.81		89.27	
Direct fixed investment	896.47		602.54	
Unexpected expenditure and contractors' fees	161.37		108.46	
Total depreciated capital	1057.84		711.00	
Land cost	21.16		14.22	
Start-up capital	105.78		71.10	
Total fixed investment	1184.78		796.32	
Working cost	177.72		119.45	
Total capital investment	1362.50		915.77	

Table 5. Variable and fixed costs of SGS [17,26,47].

Items	Cost
Variable cost	
Biomass (CNY/t)	289.05
Industrial water (CNY/t)	5.00
Catalysts in F-T reaction (CNY/kg)	215.74
Catalysts in gas-water shift reaction (CNY/kg)	124.36
Catalysts in hydrocracking (CNY/kg)	350.32
PSA padding (CNY/kg)	31.09

Fixed cost	
Workers (three-shift)	120
Annual pay (CNY/y)	150,000
Insurance and local taxes	27.24[a]
Operation and maintenance	27.24[a]

Where a is calculated as $2\% C_{TFI}$ which represents the total fixed investment introduced in Appendix Table A2.

3.3.5 Cost of liquid fuel products

The fuel cost is one of the primary indicators for technical economic evaluation of the system, which was calculated as follows. Under the condition that the net present value (NPV) is not less than 0 and the internal rate of return (IRR) is not less than the discount rate, the minimum price of the fuel products is taken as the fuel cost. The NPV and IRR will be calculated based on the annual net cash flow C_n as follows [48]:

$$NPV=\sum_{n=0}^{N}\frac{C_n}{(1+i_0)^n} \tag{31}$$

$$\sum_{n=0}^{N}\frac{C_n}{(1+IRR)^n}=0 \tag{32}$$

Where the C_n is the annual net cash flow of n th year; i_0 is discount rate; N represents the system designed life. The economic assumptions used in the NPV calculation are shown in Table 6.

Table 6. Economic assumptions

Economic assumptions	Contents
System designed life (year)	30
Loan interest rate	8.00%

Loan proportion	100.00%
Depreciation method	Linear depreciation without salvage value
Construction period (year)	3
Capital input in the first three years	0
First year	50% C_{TFI}
Second year	30% C_{TFI}
Third year	20% C_{TFI}
Discount rate	5.00%
Tax rate	33.00%

3.4 Ecological indicator

3.4.1 Methodology for calculating

The carbon emission or water consumption defined as EI_{total} is considered as a sum of EI_{direct} and $EI_{indirect}$, which described as [49]:

$$EI_{total} = EI_{direct} + EI_{indirect} \tag{33}$$

where the EI_{direct} is direct carbon emission or water consumption, and $EI_{indirect}$ is indirect carbon emission or water consumption. The EI_{direct} refers to the emission or the consumption from natural source and can be expressed as the sum of $EI_{direct,i}$ [49]:

$$EI_{direct} = \sum EI_{direct,i} \tag{34}$$

Where the $EI_{direct,i}$ refers to the direct emission or the consumption for each part of the system. The $EI_{indirect}$ can be also expressed as the sum of $EI_{indirect,i}$ and further expressed as [49]:

$$EI_{indirect} = \sum EI_{indirect,i} = \sum C_i I_i \tag{35}$$

where the $EI_{indirect,i}$ represents each products' emission or consumption, and C_i is the cost of each products based on the previously estimation of cost of the systems, and I_i (t CO_2 eq/10^4CNY or m^3/10^4CNY) is the appropriate sectoral embodied industry intensity of each products' emission or consumption referring to the Environmental input-output database in China [50].

Carbon emission and water consumption data are converted into carbon footprint and water footprint for further analysis of its impacts on environment. The LHV of gasoline and diesel was used as a unified evaluation standard to calculate the carbon footprint and water footprint of the two systems at different processes.

3.4.2 CO_2 Emission and water consume of faming and transportation

The method introduced above are not suitable for calculating those footprints of faming and transportation sections of raw materials, so another method is applied. The distribution coefficient of stalk i is the ratio of the market value of stalk per unit cultivated area to the sum of the market value of both cotton and stalk per unit cultivated area. According to the investigation, the average market price of cotton in Xinjiang China is 12736 CNY/t, while the price of cotton stalk is 290 CNY/t [21]. Together with the cotton yield data, the yield of cotton stalk per unit cultivated area is about 4.5 times of that of cotton, and the distribution coefficient i is 0.093 in this case. The data of price and yield are attached in the Appendix, Table A3 and A4 [51]. The carbon emission and the water consumption of cotton stalk were 0.28 kg CO_2 eq /kg and 0.45 m^3 /kg respectively. They were calculated by multiplying the distribution coefficient of stalk i and the carbon emission or the water consumption of the whole

cotton plant including its stalk in Xinjiang China, which were 2.98 kg CO_2 eq /kg [52] and 4.8 m^3 /kg [53] respectively.

The distribution density of cotton straws in Xinjiang is 9.84t /km^2 [54]. According to the annual biomass consumption of SGS and reference system, the collection radius of cotton straws is 43km and 54km respectively. Due to the lack of relevant data support, the transport process of raw materials was simplified as carrying biomass from the collection area to the factory. Assuming the fuel used by agricultural transport vehicles is diesel, the consumption coefficient of diesel during transport is $0.05\,L/(t\cdot km)$ [55]. According to the material flow calculated previously and the density of diesel taken as 0.83kg/L, it was calculated that the diesel consumed by SGS and the reference system in the transportation process is 102t and 203t respectively, which results in the direct CO_2 emission of two systems accounting for 0.31×10^2 t/y and 0.62×10^3 t/y respectively. The farming and transportation data of CO_2 emission and water consumption of two systems are presented in Table 7.

Table 7. The CO_2 emission and water consumption of two systems

	SGS		Reference system	
	Diesel	Straw	Diesel	Straw
Section number	37		37	
Direct CO_2 emission (t/y)	0.31E+03		0.62 E+03	
Indirect CO_2 emission Intensity (t/10^4CNY)	1.09E+01		1.09E+01	
Water consumption intensity (m^3/10^4CNY)	7.08E+01		7.08E+01	
Value (10^4CNY/y)	7.73E+01		1.65E+02	

CO_2 emission (t/y)	1.15E+03	1.68E+04	2.46E+03	2.84E+04
Water consumption (m^3/y)	5.47E+03	2.52E+07	1.17E+04	4.18E+07

4. Result and discussion

4.1 Energy performance

Table 8 shows the energy and the exergy efficiency of two systems. It presents almost the same energy efficiency of 40.66% for SGS and 40.22% for reference system. While the exergy efficiency of SGS is higher than that of reference system, accounting for 41.35% and 38.35%, respectively. The replacement of the solar energy and relative devices made little promotion for the energy efficiency of SGS. But solar gasification could still be regarded as a more appropriate utilization of bio-energy for its better exergy efficiency.

According to the material flow calculated by Aspen Plus, each parts' thermal loss and exergy loss of SGS have been presented in Fig 7. The attenuation of solar energy failed to be received by the mirrors may be responsible for the biggest energy and exergy loss of solar collector, which accounting for 31.81% and 29.46% respectively. Though the optical loss is unable to be eliminated, it can be alleviated by redesigning the heliostat field with a higher efficiency. Besides, we can reduce the fuel demand for the power generation and improve the thermal efficiency of the system by using the heat from the FT reaction to preheat the working fluid in the power generation section. What's more, after analyzing the power consumption inside the system, it is found water electrolyser takes the largest power consumption proportion, accounting for 54.74%, which indicates that increasing the efficient of the hydrogen production

process is the most effective way to reduce the power consumption inside the system and thus improve the energy efficiency.

Table 8. The thermal efficiency and exergy efficiency of two systems.

System	SGS		Reference system	
	Energy	Exergy	Energy	Exergy
Input (kW)				
Biomass (kW)	17565.00	19822.17	17565.00	19822.17
Solar energy (kW)	11235.24	10647.56		
Output (kW)				
Gasoline (kW)	6837.44	7350.65	4125.36	4435.00
Diesel (kW)	4872.85	5247.69	2940.03	3166.19
Efficiency (%)	40.66	41.35	40.22	38.35
Electricity				
Air separation (kW)			469.75	
CO_2 removal (kW)	273.04		253.71	
Compressor (kW)	861.72		533.62	
Water electrolyser (kW)	1372.26		827.95	

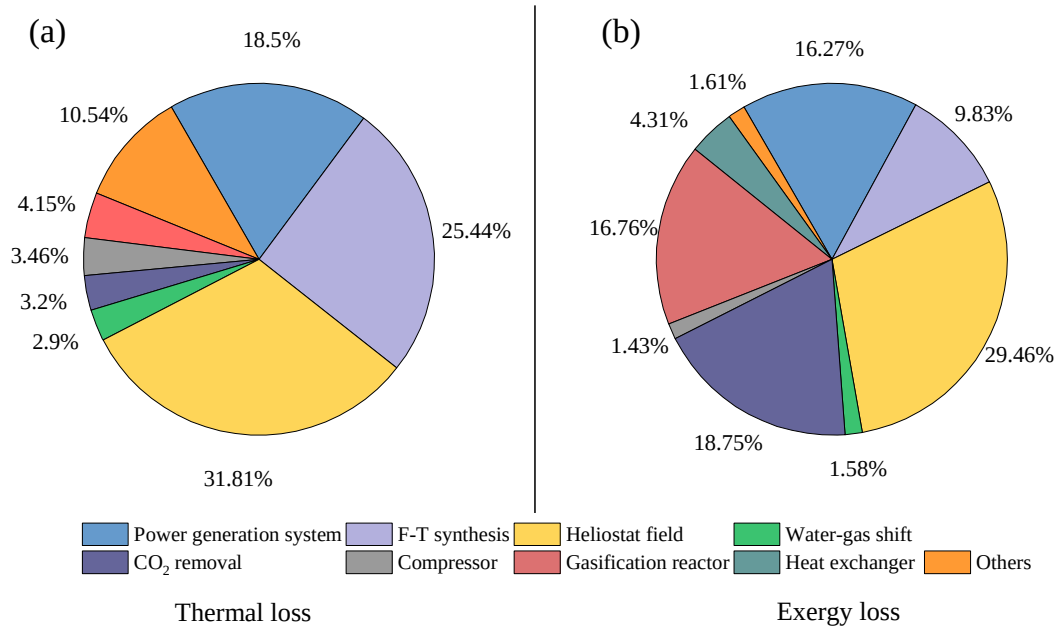

Fig 7. The thermal loss and exergy loss proportion of SGS each part:

(a) Thermal loss; (b) Exergy loss

The efficiency and the productivity of SGS changes with different biomass feedstock input. Table 9 shows the compositions of six different biomasses as well as the material flow and efficiency of SGS fed with these feedstocks. The fuel productivity changes along with the total input of water, which corresponds with the theoretical results calculated by Eq 6. As shown in Fig 8, both the thermal and exergy efficiency present a strong correlation with the standard molar enthalpy of formation (h, kJ/mol) of each feedstock and their volatiles content (V, wt%). The Bio-1 has a higher h and V, resulting its highest efficiency. While in the Bio-3, the lowest h and V corresponded to the lowest efficiency. The Bio-6 have the highest V, but its efficiency of thermal and exergy were less than those of bio-1 because of its lower h. According to Eq 11, the total heat absorption of the gasification reaction ($\Delta h_{gasification,T}$) is negatively correlated with the h. And the decrease of the total heat absorption caused

by the lower h can reduce the demand of solar energy input, which eventually leads to an efficiency increment. Higher volatile fraction is reported to have a potential of higher syngas productivity and higher H_2 fraction [34,56]. What's more, the volatile fraction generally predicts the heating value of feedstock [57], which would affect the h. Thus, to some extends, the h and V shows the same influence on the efficiency of the SGS.

Table 9. Characterization of six feedstocks [13,58–61] and the material flow as well as efficiency of SGS fed with these feedstocks

Biomass	Number	Bio-1	Bio-2	Bio-3	Bio-4	Bio-5	Bio-6
	Material	Cotton stock-1	Cotton stock-2	Rice husk	Corn stover-1	Corn stover-2	Corn stover-3
C (wt%)		45.01	46.56	50.03	45.70	43.60	46.09
H (wt%)		6.09	6.04	6.07	5.70	6.30	5.60
O (wt%)		40.04	41.82	42.54	42.36	48.30	38.22
V (wt%)		80.79	77.49	68.32	75.03	75.70	80.92
Bio (kg/s)		1	1	1	1	1	1
H_2O (kg/s)		0.525	0.530	0.577	0.522	0.390	0.590
Fuel (kg/s)		1.536	1.541	1.588	1.533	1.399	1.601

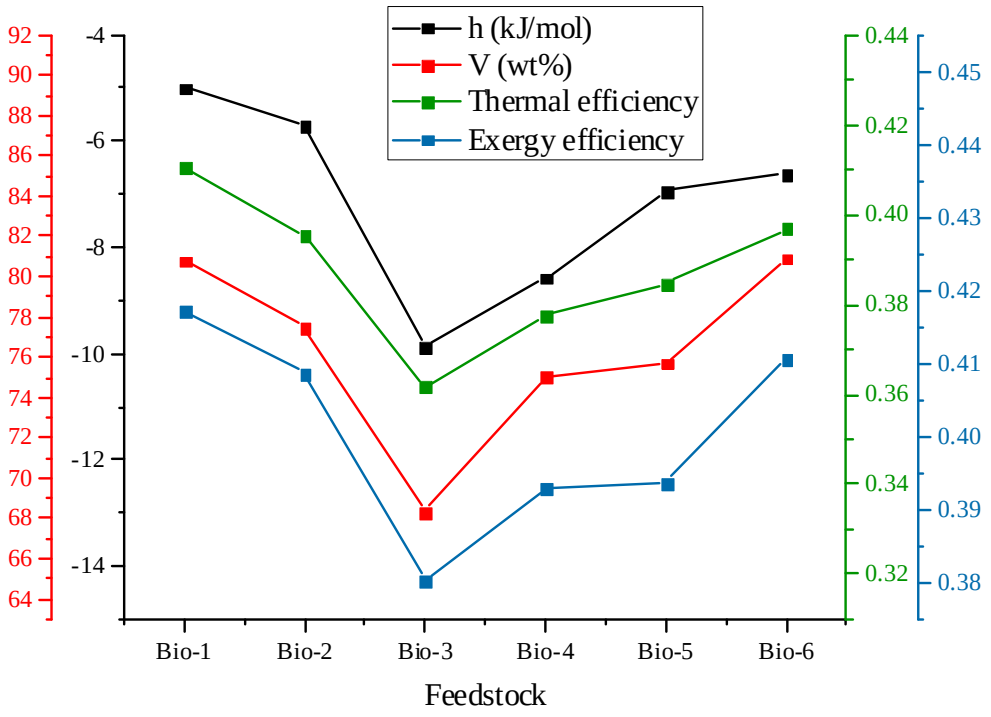

Fig 8. The standard molar enthalpy of formation and the volatiles content of six feedstocks and the efficiency of SGS fed with these feedstocks.

The Fig 9 shows the effect of DNI to the SGS system. Both the thermal and exergy efficiency have a peak when DNI reaches 600 W/m^2. However, the syngas productivity continually increases along with the DNI and tends to be stable as DNI >700 W/m^2, which is set as the nominal operation point of SGS for a higher yield of syngas. According to the data in Table 2, the SGS produced 49.44% more refined syngas and 65.74% more liquid fuels than the reference system, indicating that the SGS has huge advantage in productivity because the feedstock can be highly utilized instead of being consumed to provide reaction heat. However, this advantage could be narrowed when the DNI is lower than the nominal point, and will be eliminated as DNI decreasing to 335 W/m^2, which was called equilibrium point in this paper.

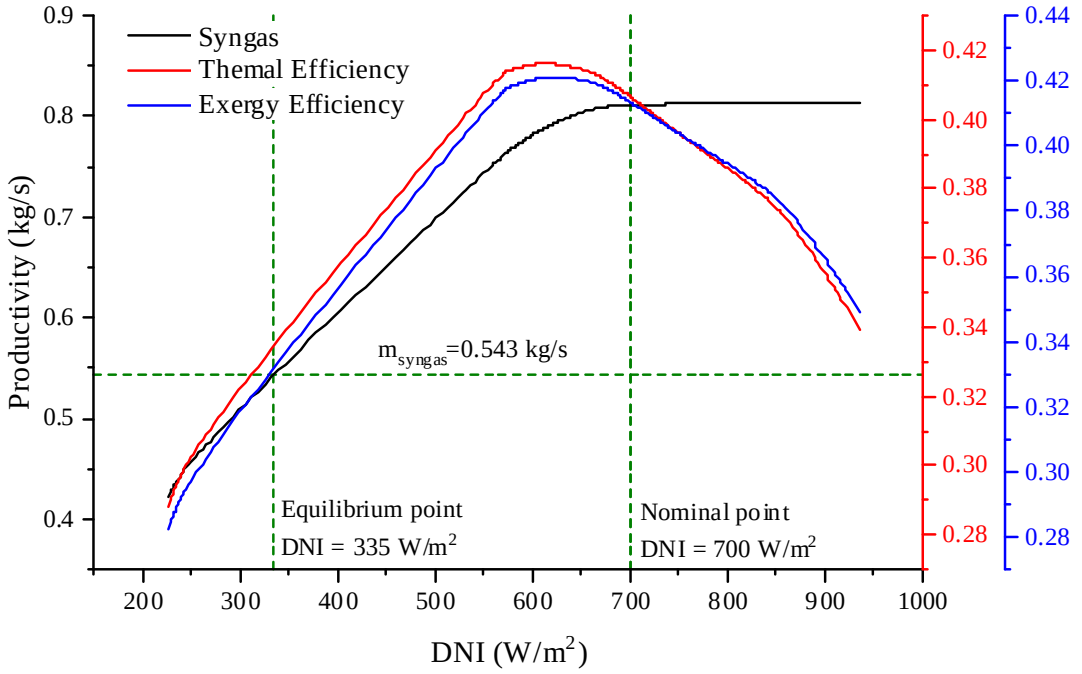

Fig 9. The productivity and efficiencies of SGS in different DNI

4.2 Economic analysis

As shown in Table 4, fuel synthesis takes the largest part of equipment expenditure both in SGS and reference systems, reaching 36.37% and 54.11% respectively. The SGS and reference system have their own unique equipment such as solar collector and air separator. The cost of syngas storage tanks in SGS is 22.5 times of that in reference system. Because SGS needs bigger and more tanks to store the syngas to deal with the transience of solar energy and avoid the system instability that would make the downstream syngas supply discontinued. In this case, more syngas compressors are needed in SGS, so the cost of auxiliary equipment of the SGS is 52.64% higher than that of the reference system. With the same output of refined syngas, SGS consumes less biomass feedstock and requires less crude syngas to be refined. Therefore, the solar energy system has a smaller size of equipment used for

syngas production, and the cost is 59.98% of the reference system. The results of the investment schedule show that the equipment cost of fuel synthesis, syngas storage and solar collector takes the highest proportion in the cost of fundamental equipment. Further optimization improvement of these three parts could effectively control and reduce the investment of the system. For example, a lower solar multiply could increase the utilization rate of this part of equipment and cut down the cost of storage tanks due to the less demand of syngas stored for fuel synthesis at night, which contributes to reducing the production cost and improving the production capacity of the system.

The main economic performance of each system is shown in Table 4. The total investment of solar energy system is 48.78% higher than that of the reference system with the same production capacity. In the case of similar NPV and IRR, the production costs of SGS for gasoline and diesel are 1.507×10^4 CNY/t and 1.242×10^4 CNY/t respectively, which is 24.32% higher than the production costs of the reference system. According to Summary of gasoline and diesel retail prices in 36 large and medium-sized cities in China in October 2018 [62,63], the price of gasoline (#92) was 1.045×10^4 CNY/t, while the price of diesel (#0) was 0.880×10^4 CNY/t. Taking these as the reference prices, the cost of producing liquid fuel from biomass in both systems is much higher than that producing from oil (costing 44.21% more for SGS, and 16.30% for reference systems). However, in the perspective of energy sustainability, the continuous depletion of fossil resource will inevitably lead to the rise of oil price, and the cost of solar energy system can be further reduced through

technological progress and optimized design of system process. All of these indicate that SGS has potential for a long-term competition.

As a party for the United Nations Framework Convention on Climate Change, the carbon tax is inevitable in order to meet the goal of controlling greenhouse gas emissions. Since a reference system releases more greenhouse gas per unit LHV of products than SGS, the carbon tax would have a bigger impact on the reference system. Take the cost of producing gasoline as an example. When the carbon tax reached 551.42 CNY/t, the production cost of SGS increased by 14.62%, reaching 2204.38 CNY/t, while the production cost of the reference system increased by 42.49%, reaching 5152.44 CNY/t. The production cost of the two systems come to the same level in this case. A further increase of the carbon tax would bring SGS economic advantage immediately.

To further analyze and determine the factors that have the great impact on system cost, the variation of cost under 13 scenarios set in a range of ±20% has been estimated, and the results are presented in Fig 10. It shows that the production capacity and the proportion of loans has the biggest influence on the system cost. With the production capacity increasing by 20%, the total cost of SGS is reduced by 15.4%. It proves that technological progress or process optimization can cut down the cost by improving system capacity with little investment increase. In scenario 9, the proportion of loans in the total investment of the system is reduced to 80%, and the system cost is reduced by 12.241%, making it the second biggest influence factor to system cost. The total system cost seems to be less sensitive to the changes of

equipment cost, interest rate of loan and the fixed cost, which cause the variation of total cost less than 7%. The changes of revenue tax rate and price of biomass have nearly no influence (less than 1.6%) on the total cost.

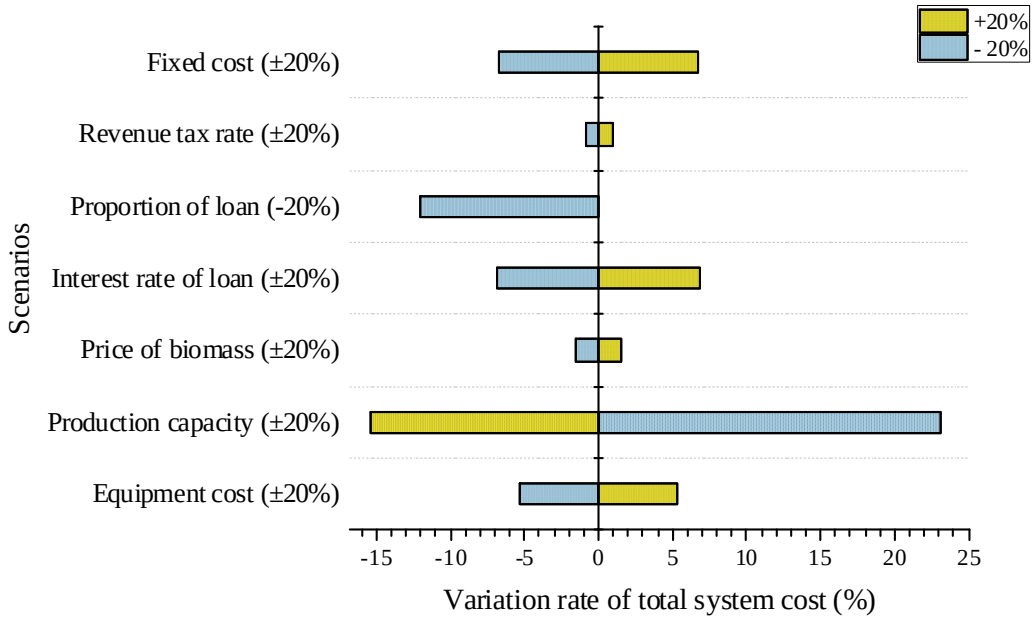

Fig 10. Variation rate of total system cost under 13 scenarios.

4.3 Ecological analysis

The carbon and the water footprint of two systems are given in Table 10 and 0. Overall, the carbon footprint of SGS and the reference system is 0.1561 t/GJ and 0.2825 t/GJ respectively. And their water footprint is 39.514 m^3/GJ and 64.416 m^3/GJ respectively. The carbon and water footprints of SGS were only 55.27% and 61.34% of those of the reference system, indicating that SGS has a better ecology performance.

Table 10. Carbon footprint of two systems

System	Processes	CO_2 emission (t/y)	Direct carbon footprint (t/GJ)	Indirect carbon footprint (t/GJ)	Life-cycle carbon footprint (t/GJ)

SGS	Farming	1.57E+04	0.0000	0.0237	0.0237
	Transportation of biomass	1.15E+03	0.0005	0.0013	0.0017
	Building and equipment	2.50E+04	0.0000	0.0379	0.0379
	Operation and maintenance	6.14E+04	0.0865	0.0063	0.0928
	Sum up	1.03E+05	0.0870	0.0691	0.1561
Reference system	Farming	2.60E+04	0.0000	0.0392	0.0392
	Transportation of biomass	2.46E+03	0.0010	0.0027	0.0037
	Building and equipment	1.63E+04	0.0000	0.0246	0.0246
	Operation and maintenance	1.42E+05	0.2023	0.0126	0.2149
	Sum up	1.87E+05	0.2033	0.0792	0.2825

Table 11. Water footprint of two systems

System	Processes	Water consumption (m^3/y)	Direct water footprint (m^3/GJ)	Indirect water footprint (m^3/GJ)	Life-cycle water footprint (m^3/GJ)
SGS	Farming	2.52E+07	35.723	2.373	38.097
	Transportation of biomass	5.47E+03	0.000	0.008	0.008
	Building and equipment	3.32E+05	0.000	0.502	0.502
	Operation and maintenance	6.00E+05	0.801	0.106	0.907

	Sum up	2.61E+07	36.524	2.990	39.514
Reference system	Farming	4.18E+07	59.208	3.934	63.142
	Transportation of biomass	1.17E+04	0.000	0.018	0.018
	Building and equipment	2.08E+05	0.000	0.314	0.314
	Operation and maintenance	6.24E+05	0.730	0.213	0.943
	Sum up	4.26E+07	59.938	4.478	64.416

In farming process, the carbon footprint of SGS and reference system are 0.0237 t/GJ and 0.0392 t/GJ, respectively. Their water footprints are 38.097 m^3/GJ and 63.142 m^3/GJ, respectively. The carbon footprint of SGS during this process is 39.67% lower than that of the reference system benefiting from the more efficient utilization of feedstock. Water consumption in this process accounted for 96.41% and 98.02% of the total water consumption of two systems, respectively. Generally, it is common for bio-energy technology that farming process consumes the largest part of water. But it should be clarified that the extremely high water consumption ratio of two systems is related to the arid climate in Xinjiang instead of technological disadvantages of biomass utilization itself. Besides, the more efficient utilization of feedstock also results in a 46.87% lower carbon footprint and water footprint of SGS in biomass transportation process than that of reference system.

In the building and equipment section, the carbon footprint of SGS is 0.0379t /GJ, 53.76% higher than that of reference system; and the water footprint is 0.502m3 /GJ, 59.96% higher than that of reference system. This is because the SGS needs to build solar collectors and larger-scale gas storage devices, which brings additional indirect

carbon and water footprint.

The operation and maintenance process contribute the largest proportion of whole carbon footprint in both systems, which is shown in Table 10. The carbon footprint of SGS in this process is 43.2% of that of reference system, because the reference system has additional carbon emission derived from burning part of feedstock. The distribution of carbon emission in this process (Fig 11) shows the CO_2 removal process is the major source of carbon emission. Moreover, SGS produced liquid fuels with less electricity and catalyst consumption per LHV than reference systems. The CO_2 removal process of reference system release 166% more CO_2 than that of SGS because it needs more biomass input as the liquid fuel products are set to be the same for two system, which would obviously increase the amount of CO_2. At the meantime, part of the feedstock in reference system is combusted to provide the heat, which makes a further increase of the amount of CO2 in the crude syngas. The air separator that only exists in reference system is the major reason for the higher electricity consumption afforded by power generation sector. And the higher CO_2 concentration in the syngas results in the more electricity consumption of CO_2 removal devices. These together lead to the higher CO_2 emission from power generation by combustion. As for the catalysts used in water-gas-shift reaction, FT synthesis and hydrocracking process, the amount of the catalysts is determined by the flow rate of the syngas. So with the same fuel productivity, the SGS needs less syngas and thus has a lower indirect CO_2 emission from catalysts. As for the water footprint, although the direct water footprint of SGS is higher than that of reference system due to the additional

water used in gasification process to increase the H_2/CO ratio, the indirect water footprint caused by using catalyst and other materials is much lower than that of the reference system. This leads to the overall water footprint of SGS during operation and maintenance process is still smaller than a reference system.

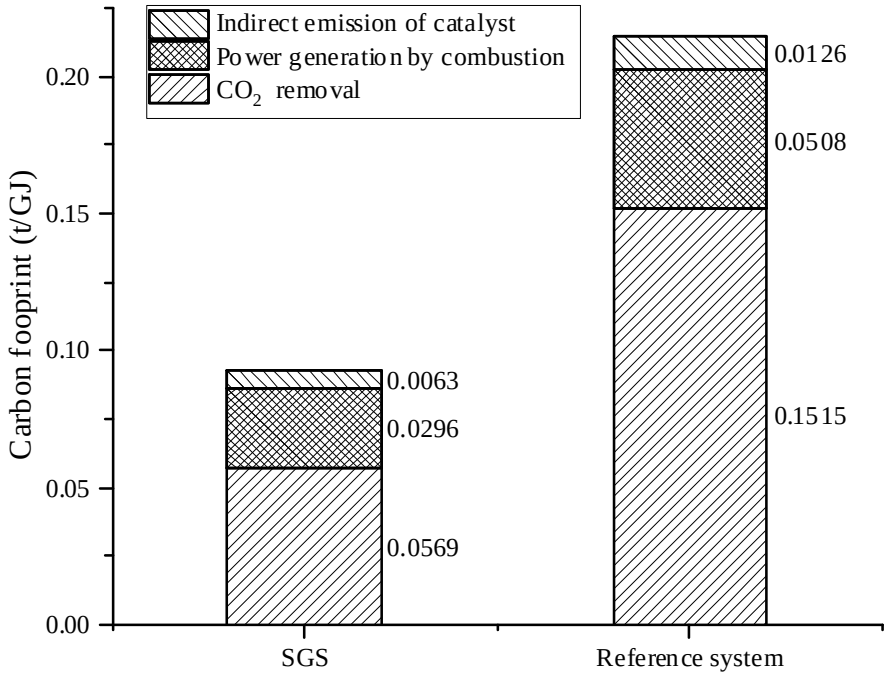

Fig 11. Distribution of carbon emission in operation and maintenance process

5. Conclusion

Solar gasification system (SGS) produced 49.44% more refined syngas and 65.74% more liquid fuels than the reference system. The thermal efficiency of the two systems was about the same, while the exergy efficiency of the SGS was slightly higher than that of the reference system. The volatile matter fraction and standard mole enthalpy of feedstock formation are positively related to the thermal and exergy efficiency of SGS. The efficiencies reach their maximum value at the DNI of 600W/m^2, and the productivity continually increases and finally remain unchanged as DNI>700 W/m^2. Though the SGS are not economic-competitive in short term, it still

has potential when the carbon tax reaches 551.42 CNY/t. It's proven that the change of production capacity has a great influence on system cost, whose changes of ±20% could lead to a system cost change rate ranging from -15.406% to 23.109%. The total carbon and water footprints of the solar system were only 55.27% and 61.34% of those of the reference system, showing that SGS has a better ecology performance.

Acknowledgement

Authors acknowledge funding from the National Natural Science Foundation of China (51706083), International Cooperation Project of Shenzhen (GJHZ20190820102607238), Natural Science Foundation of Shenzhen (JCYJ20170818164006890) and the Key Laboratory of Coal Science and Technology, Taiyuan University of Technology (MKX201905).

.

Reference

[1] Bp 2019 Energy Outlook. 2019.

[2] Ruiz JA, Juárez MC, Morales MP, Muñoz P, Mendívil MA. Biomass gasification for electricity generation: Review of current technology barriers. Renew Sustain Energy Rev 2013;18:174–83. https://doi.org/10.1016/j.rser.2012.10.021.

[3] Service RF. Biomass Fuel Starts to See the Light. Science (80-) 2009;326:1474–1474. https://doi.org/10.1126/science.326.5959.1474.

[4] Parthasarathy P, Narayanan KS. Hydrogen production from steam gasification of biomass: Influence of process parameters on hydrogen yield - A review. Renew Energy 2014;66:570–9. https://doi.org/10.1016/j.renene.2013.12.025.

[5] Dry ME. The Fischer-Tropsch process: 1950-2000. Catal. Today, vol. 71, Elsevier; 2002, p. 227–41. https://doi.org/10.1016/S0920-5861(01)00453-9.

[6] Nickerson TA, Hathaway BJ, Smith TM, Davidson JH. Economic assessment of solar and conventional biomass gasification technologies: Financial and policy implications under feedstock and product gas price uncertainty. Biomass and Bioenergy 2015;74:47–57. https://doi.org/10.1016/j.biombioe.2015.01.002.

[7] Iliuta I, Leclerc A, Larachi F. Allothermal steam gasification of biomass in cyclic multi-compartment bubbling fluidized-bed

gasifier/combustor - New reactor concept. Bioresour Technol 2010;101:3194–208. https://doi.org/10.1016/j.biortech.2009.12.023.

[8] Piatkowski N, Wieckert C, Weimer AW, Steinfeld A. Solar-driven gasification of carbonaceous feedstock - A review. Energy Environ Sci 2011;4:73–82. https://doi.org/10.1039/c0ee00312c.

[9] Taylor RW, Berjoan R, Coutures JP. Solar gasification of carbonaceous materials. Sol Energy 1983;30:513–25. https://doi.org/https://doi.org/10.1016/0038-092X(83)90063-4.

[10] Lédé J. Solar thermochemical conversion of biomass. Sol Energy 1999;65:3–13. https://doi.org/10.1016/S0038-092X(98)00109-1.

[11] Zedtwitz P v., Steinfeld A. The solar thermal gasification of coal — energy conversion efficiency and CO2 mitigation potential. Energy 2003;28:441–56. https://doi.org/10.1016/S0360-5442(02)00139-1.

[12] Kaniyal AA, Van Eyk PJ, Nathan GJ, Ashman PJ, Pincus JJ. Polygeneration of liquid fuels and electricity by the atmospheric pressure hybrid solar gasification of coal. Energy and Fuels 2013;27:3538–55. https://doi.org/10.1021/ef400198v.

[13] Hathaway BJ, Honda M, Kittelson DB, Davidson JH. Steam gasification of plant biomass using molten carbonate salts. Energy 2013;49:211–7. https://doi.org/10.1016/j.energy.2012.11.006.

[14] Hathaway BJ, Kittelson DB, Davidson JH. Integration of Solar Gasification With Conventional Fuel Production: The Roles of Storage

and Hybridization. J Sol Energy Eng 2014;136. https://doi.org/10.1115/1.4025971.

[15] Yang SY, Li B xia., Zheng J wei., Kankala RK. Biomass-to-Methanol by dual-stage entrained flow gasification: Design and techno-economic analysis based on system modeling. J Clean Prod 2018;205:364–74. https://doi.org/10.1016/j.jclepro.2018.09.043.

[16] Dimitriou I, Goldingay H, Bridgwater A V. Techno-economic and uncertainty analysis of Biomass to Liquid (BTL) systems for transport fuel production. Renew Sustain Energy Rev 2018;88:160–75. https://doi.org/10.1016/j.rser.2018.02.023.

[17] Rahbari A, Shirazi A, Venkataraman MB, Pye J. A solar fuel plant via supercritical water gasification integrated with Fischer–Tropsch synthesis: Steady-state modelling and techno-economic assessment. Energy Convers Manag 2019;184:636–48. https://doi.org/10.1016/j.enconman.2019.01.033.

[18] Loutzenhiser PG, Muroyama AP. A review of the state-of-the-art in solar-driven gasification processes with carbonaceous materials. Sol Energy 2017;156:93–100. https://doi.org/10.1016/j.solener.2017.05.008.

[19] Bai Z, Liu Q, Lei J, Li H, Jin H. A polygeneration system for the methanol production and the power generation with the solar-biomass thermal gasification. Energy Convers Manag 2015;102:190–201. https://doi.org/10.1016/j.enconman.2015.02.031.

[20] Pala LPR, Wang Q, Kolb G, Hessel V. Steam gasification of biomass with subsequent syngas adjustment using shift reaction for syngas production: An Aspen Plus model. Renew Energy 2017;101:484–92. https://doi.org/10.1016/j.renene.2016.08.069.

[21] Bai Z, Jin HG, Liu QB. Integration Mechanism for Thermochemical Hybrid Utilization for Solar Energy and Biomass. Institute of Engineering Thermophysics, Chinese Academy of Sciences, 2016.

[22] Müller F, Poživil P, van Eyk PJ, Villarrazo A, Haueter P, Wieckert C, et al. A pressurized high-flux solar reactor for the efficient thermochemical gasification of carbonaceous feedstock. Fuel 2017;193:432–43. https://doi.org/10.1016/j.fuel.2016.12.036.

[23] Ng YC, Lipiński W. Thermodynamic analyses of solar thermal gasification of coal for hybrid solar-fossil power and fuel production. Energy 2012;44:720–31. https://doi.org/10.1016/j.energy.2012.05.019.

[24] McLean C. Energy efficiency of gas separation by pressure swing adsorption. The University of British Columbia, 1994.

[25] Selvatico D, Lanzini A, Santarelli M. Low Temperature Fischer-Tropsch fuels from syngas: Kinetic modeling and process simulation of different plant configurations. Fuel 2016;186:544–60. https://doi.org/https://doi.org/10.1016/j.fuel.2016.08.093.

[26] Swanson RM, Platon A, Satrio JA, Brown RC. Techno-economic

analysis of biomass-to-liquids production based on gasification. Fuel 2010;89:S11–9. https://doi.org/https://doi.org/10.1016/j.fuel.2010.07.027.

[27] Guo P, Van Eyk PJ, Saw WL, Ashman PJ, Nathan GJ, Stechel EB. Performance assessment of Fischer-Tropsch liquid fuels production by solar hybridized dual fluidized bed gasification of lignite. Energy and Fuels 2015;29:2738–51. https://doi.org/10.1021/acs.energyfuels.5b00007.

[28] Suárez París R, L'Abbate ME, Liotta LF, Montes V, Barrientos J, Regali F, et al. Hydroconversion of paraffinic wax over platinum and palladium catalysts supported on silica–alumina. Catal Today 2016;275:141–8. https://doi.org/10.1016/j.cattod.2015.11.026.

[29] Lei Q, Wang B, Wang P, Liu S. Hydrogen generation with acid/alkaline amphoteric water electrolysis. J Energy Chem 2019;38:162–9. https://doi.org/https://doi.org/10.1016/j.jechem.2018.12.022.

[30] Chen L, Luo J, Sun F, Wu C. Design efficiency optimization of one-dimensional multi-stage axial-flow compressor. Appl Energy 2008;85:625–33. https://doi.org/10.1016/j.apenergy.2007.10.003.

[31] Danish SN, Qureshi SR, Imran MM, Khan SUD, Sarfraz MM, El-Leathy A, et al. Effect of tip clearance and rotor-stator axial gap on the efficiency of a multistage compressor. Appl Therm Eng 2016;99:988–95. https://doi.org/10.1016/j.applthermaleng.2016.01.132.

[32] Zhang XT, Tan TW, Chang J. Study on Catalysts and Technology of Methanol Synthesis from Biomass Syngas. Beijing University of

Chemical Technology, 2005.

[33] Chen ZW, Gao L. Analyses on supercritical water gasification of coal and integration of novel ower generation systems. Institute of engineering thermophysics, Chinese Academy of Sciences, 2018.

[34] Li YY, Xiong YM, Yang YP. The Energy Efficiency Optimization and Feedwater Control Analysis of Integrated Solar Combined Cycle. J Eng Thermophys 2019;40:1–9.

[35] Bellouard Q, Abanades S, Rodat S, Dupassieux N. Solar thermochemical gasification of wood biomass for syngas production in a high-temperature continuously-fed tubular reactor. Int J Hydrogen Energy 2017;42:13486–97. https://doi.org/10.1016/j.ijhydene.2016.08.196.

[36] Hathaway BJ, Kittelson DB, Davidson JH. Development of a Molten Salt Reactor for Solar Gasification of Biomass. Energy Procedia 2014;49:1950–9. https://doi.org/10.1016/j.egypro.2014.03.207.

[37] Chuayboon S, Abanades S, Rodat S. Insights into the influence of biomass feedstock type, particle size and feeding rate on thermochemical performances of a continuous solar gasification reactor. Renew Energy 2019;130:360–70. https://doi.org/10.1016/j.renene.2018.06.065.

[38] Muroyama A, Shinn T, Fales R, Loutzenhiser PG. Modeling of a Dynamically-Controlled Hybrid Solar/Autothermal Steam Gasification Reactor. Energy & Fuels 2014;28:6520–30. https://doi.org/10.1021/ef501535r.

[39] He Q, Luo N, Liu WY. Economic analysis of gas storage devices for compressed air energy storage system based on life cycle cost. Chem Ind Eng Prog 2018;37:67–74.

[40] Xiang SB, Huang Y. Shell-and-tube heat exchanger network total cost optimization using improved particle swarm algorithm. J Heilongjiang Univ Sci & Technol 2015;25:115–8. https://doi.org/10.3969/j.issn.2095-7262.2015.01.024.

[41] Feng J, Ni WD, Sugishita H, Wang LM, Li Z. Simulation and economic analysis of IGCC power plant. Gas Turbine Technol 2006:25–9. https://doi.org/10.16120/j .cnki .issn1009 -2889.2006.02.005.

[42] Wu Y, Feng J, Li W. System development of integrated high temperature and low temperature Fischer–Tropsch synthesis for high value chemicals. Chem Eng Res Des 2018;131:80–91. https://doi.org/10.1016/j.cherd.2017.12.008.

[43] Haarlemmer G, Boissonnet G, Peduzzi E, Setier P-A. Investment and production costs of synthetic fuels – A literature survey. Energy 2014;66:667–76. https://doi.org/10.1016/j.energy.2014.01.093.

[44] Larson ED, Jin H, Celik FE. Large-scale gasification-based coproduction of fuels and electricity from switchgrass. Biofuels, Bioprod Biorefining 2009;3:174–94. https://doi.org/10.1002/bbb.137.

[45] Baliban RC, Elia JA, Floudas CA. Toward Novel Hybrid Biomass, Coal, and Natural Gas Processes for Satisfying Current Transportation

Fuel Demands, 1: Process Alternatives, Gasification Modeling, Process Simulation, and Economic Analysis. Ind Eng Chem Res 2010;49:7343–70. https://doi.org/10.1021/ie100063y.

[46] Schmidt O, Gambhir A, Staffell I, Hawkes A, Nelson J, Few S. Future cost and performance of water electrolysis: An expert elicitation study. Int J Hydrogen Energy 2017;42:30470–92. https://doi.org/https://doi.org/10.1016/j.ijhydene.2017.10.045.

[47] National Bureau of Statistic. China Statistical Yearbook-2019. Beijing: China Statistic Press; 2019.

[48] Yang Q, Zhou H, Zhang X, Nielsen CP, Li J, Lu X, et al. Hybrid life-cycle assessment for energy consumption and greenhouse gas emissions of a typical biomass gasification power plant in China. J Clean Prod 2018;205:661–71. https://doi.org/10.1016/j.jclepro.2018.09.041.

[49] Yang Q, Liang J, Li J, Yang H, Chen H. Life cycle water use of a biomass-based pyrolysis polygeneration system in China. Appl Energy 2018;224:469–80. https://doi.org/10.1016/j.apenergy.2018.05.009.

[50] Chen GQ, Chen ZM. Carbon emissions and resources use by Chinese economy 2007: A 135-sector inventory and input–output embodiment. Commun Nonlinear Sci Numer Simul 2010;15:3647–732. https://doi.org/https://doi.org/10.1016/j.cnsns.2009.12.024.

[51] Statistic Bureau of Xinjiang Uygur Autonomous Region. Xinjiang Yearbook 2017. Beijing: China Statistic Press; 2017.

[52] Zhao Y, Li Q, Hou X, Si T, Wang M, Wamg Y, et al. Study on Carbon Footprint of Cotton/Peanut Intercropping in Xinjiang. J Peanut Sci 2019:61–5.

[53] Zhong Q, Xue J, Jin Q, Gui D, GAo X, Zeng F. Water footprints of primary crop production in Xinjiang. Agric Research Arid Areas 2018;36:243–9. https://doi.org/10.7606/j.issn.1000-7601.2018.06.36.

[54] Zhang C, Qiong MA, Wang P. Estimation and utilization of the cotton straw resource in Xinjiang. J Arid L Resour Environ 2016. https://doi.org/10.13448/j.cnki.jalre.2016.219.

[55] Yang Q, Chen GQ. Greenhouse gas emissions of corn–ethanol production in China. Ecol Modell 2013;252:176–84. https://doi.org/10.1016/j.ecolmodel.2012.07.011.

[56] Wieckert C, Obrist A, Zedtwitz P Von, Maag G, Steinfeld A. Syngas Production by Thermochemical Gasification of Carbonaceous Waste Materials in a 150 kW th Packed-Bed Solar Reactor. Energy & Fuels 2013;27:4770–6. https://doi.org/10.1021/ef4008399.

[57] THIPKHUNTHOD P, MEEYOO V, RANGSUNVIGIT P, KITIYANAN B, SIEMANOND K, RIRKSOMBOON T. Predicting the heating value of sewage sludges in Thailand from proximate and ultimate analyses. Fuel 2005;84:849–57. https://doi.org/10.1016/j.fuel.2005.01.003.

[58] Li J, Xie Y, Zeng K, Flamant G, Yang H, Yang X, et al. Biomass

gasification in molten salt for syngas production. Energy 2020;210:118563. https://doi.org/10.1016/j.energy.2020.118563.

[59] Li W, Wu S, Wu Y, Huang S, Gao J. Gasification characteristics of biomass at a high-temperature steam atmosphere. Fuel Process Technol 2019;194:106090. https://doi.org/10.1016/j.fuproc.2019.05.013.

[60] Hu J, Li D, Lee DJ, Zhang Q, Wang W, Zhao S, et al. Integrated gasification and catalytic reforming syngas production from corn straw with mitigated greenhouse gas emission potential. Bioresour Technol 2019;280:371–7. https://doi.org/10.1016/j.biortech.2019.02.064.

[61] Edreis EMA, Li X, Atya AHA, Sharshir SW, Elsheikh AH, Mahmoud NM, et al. Kinetics, thermodynamics and synergistic effects analyses of petroleum coke and biomass wastes during H2O co-gasification. Int J Hydrogen Energy 2020;45:24502–17. https://doi.org/10.1016/j.ijhydene.2020.06.239.

[62] gasoline prices in 36 large and medium-sized cities in China in October 2018. Econ Anal China Pet Chem Ind 2019;12:67.

[63] Diesel prices in 36 large and medium-sized cities in China in October 2018. Econ Anal China Pet Chem Ind 2019.

Appendix

Table A1. The cost of storage tank.

Pressure (bar)	Capacity (m^3)	Material type	Metal consumption (kg)	Cost (10^6 CNY)
5	1000	Q345R	260,918	230.36

Table A2. System total investment estimation method [26].

Parameter	Method
Total fundamental equipment cost	C_{TFC}
Venues preparation (C_{site})	$15\% C_{\mathrm{TFC}}$
Service facility (C_{serv})	$20\% C_{\mathrm{TFC}}$
Direct fixed investment (C_{DFI})	$C_{\mathrm{TFC}} + C_{\mathrm{site}} + C_{\mathrm{serv}}$
Unexpected expenditure and contractors' fees (C_{cont})	$18\% C_{\mathrm{DFI}}$
Total depreciated capital (C_{TDC})	$C_{\mathrm{DFI}} + C_{\mathrm{cont}}$
Land cost (C_{land})	$2\% C_{\mathrm{TDC}}$
Start-up capital (C_{startup})	$10\% C_{\mathrm{TDC}}$
Total fixed investment (C_{TFI})	$C_{\mathrm{TDC}} + C_{\mathrm{land}} + C_{\mathrm{startup}}$
Working cost (C_{WC})	$15\% C_{\mathrm{TFI}}$
Total capital investment (C_{TCI})	$C_{\mathrm{TFI}} + C_{\mathrm{WC}}$

Table A3. Cotton market price in Xinjiang China.

Region	City	Cotton price (CNY/t)
Kashi	Payzawat	13400
	Makit	11737
	Yopurga	13144
	Marabishi	14182
Bayingol	Korla	11471
	Yuli	11970
	Bugur	11737
	Tiemenguan	11471
Turpan	Toksun	14900
Ili	Kuytun	14479
Akesu	Kuqa	12656
	Xayar	11680
Average price		12736

Table A4. Planting area, yield and straw collection of cotton in Xinjiang China [51].

Year	Cotton plantation area (10^4 hm^2)	Cotton yield (10^4 t)	Stalk yield (10^4 t)
2016	215.491	430.00	1890.00
2015	227.311	409.36	1842.12
2014	242.133	429.55	1932.98
2013	171.826	351.80	1583.10
2012	172.080	353.95	1592.78
2011	163.806	289.77	1303.97
2010	146.060	247.90	1115.55
2009	140.931	252.40	1135.80
2008	166.801	301.55	1356.98
2007	178.260	290.00	1305.00

Highlights:

► 3E analysis was used to evaluate the solar gasification biofuel production system.

► Solar gasification system (SGS) exhibited higher productivity and exergy efficiency.

► The efficiency performance of SGS under different conditions were estimated.

► Carbon and water footprint of SGS were 44.73% and 38.66% lower.

► SGS will be competitive when carbon tax reaches 551.42 CNY/t.